EurJIC
European Journal of Inorganic Chemistry

Research Article
doi.org/10.1002/ejic.202200391

Chemistry Europe
European Chemical Societies Publishing

www.eurjic.org

Intermediates in Friedel-Crafts Acylation of Fumaryl Halides

Marie C. Bayer,[a] Nikolaus Greither,[a] Christoph Jessen,[a] Alexander Nitzer,[a] and Andreas J. Kornath*[a]

Dedicated to Prof. Dr. Wolfgang Schnick on the occasion of his 65th birthday

Fumaryl chloride and fluoride were reacted with different Lewis acids to synthesize the intermediates of the Friedel-Crafts acylation. The salt of the monoacyl cation $[C_4H_2FO_2]^+[Sb_3F_{16}]^-$ was obtained from the reaction of fumaryl fluoride with SbF_5 in SO_2ClF solutions. The reaction was repeated using fumaryl chloride as starting material, which reacted under halogen exchange to obtain the salt of the monoacyl cation $[C_4H_2FO_2]^+[SbCl_2F_4]^-$. In addition, the reaction of fumaryl chloride with $SbCl_5$ in SO_2ClF was studied. The covalent donor-acceptor complex $C_4H_2Cl_2O_2 \cdot 2\ SbCl_5$ was formed, containing oxygen-bonded Lewis acids. The compounds were characterized by low-temperature vibrational spectroscopy. Single-crystal X-ray structure analyses were conducted for $[C_4H_2FO_2]^+[Sb_3F_{16}]^-$ as well as for $C_4H_2Cl_2O_2 \cdot 2\ SbCl_5$. In the solid state of $[C_4H_2FO_2]^+[Sb_3F_{16}]^-$ C···O and C···F contacts are observed and the origin of these interactions is discussed by means of ESP maps and NBO analysis. The monoacyl cation is stabilized by electrostatic attraction and electron back-donation from oxygen and fluorine ligands to the positive ring-structured π-hole at the oxocarbenium center. Besides, the formation of the diacyl cation is not observed, which is based on small distances between the positive charges involving charge-charge repulsion. The great advantage of using fumaryl halides in Friedel-Crafts acylation is featured by the possibility to synthesize ketones keeping an acyl fluoride moiety.

Introduction

Controlling chemical reactions constitutes one of the highest aims of chemistry in general. To increase product yield or eliminate side reactions, a precise knowledge of the reaction mechanism and how it can be affected is needed.[1] For industry, the Friedel-Crafts acylation represents a fundamentally important organic synthesis, as it is used to produce chemical feedstock, fine chemicals, and synthetic intermediates.[2,3] In general terms the Friedel-Crafts acylation concerns the substitution of a hydrogen atom by an acyl group catalyzed by a Lewis acid.[4,5] The first stage is the interaction between the acyl halide and the Lewis acid giving an oxonium complex followed by the formation of an acylium ion, representing the acylating agent.[6] To understand the reaction mechanism in greater detail, it is of importance to investigate these key intermediates, which are illustrated in Scheme 1. As the Friedel-Crafts acylation is usually performed with acyl chlorides,[2] we examined the reaction of fumaryl chloride with different Lewis acids to generate these intermediates. Since fluorine substituents have become a prevalent and crucial drug component,[7] we were prompted to investigate the reaction behavior of fumaryl fluoride with the Lewis acid SbF_5.

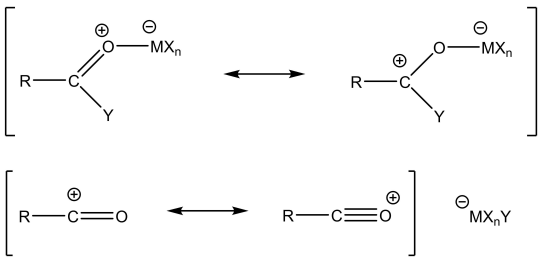

Scheme 1. Intermediates of the first step of the Friedel-Crafts acylation: Oxonium complex (top) and acylium salt (bottom).[5]

Results and Discussion

Fumaryl fluoride was reacted with SbF_5 in liquid SO_2ClF. We observe the formation of monoacylium ions according to Equation (1). It is necessary to use a very strong fluoride acceptor, such as SbF_5,[8] for the abstraction of one fluoride of $C_4H_2F_2O_2$. Attempting to synthesize the diacylium ion, twice the amount of Lewis acid was applied. However, even an eight-fold excess of SbF_5 did not result in the formation of diacyl cations.

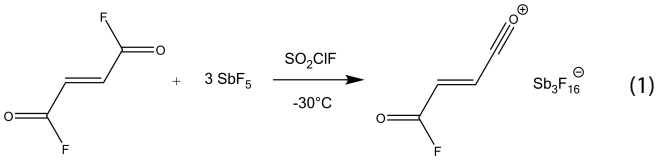

(1)

[a] M. C. Bayer, N. Greither, C. Jessen, A. Nitzer, Prof. Dr. A. J. Kornath
Department Chemie
Ludwig-Maximilians-Universität München
Butenandtstr. 5–13, (D) 81377 München, Germany
E-mail: andreas.kornath@cup.uni-muenchen.de

Supporting information for this article is available on the WWW under https://doi.org/10.1002/ejic.202200391

Research Article
doi.org/10.1002/ejic.202200391

Chemistry Europe
European Chemical Societies Publishing

To investigate the reaction behavior of the higher homologous element, fumaryl chloride was reacted with SbF_5 under the same conditions. Surprisingly, we detected the monoacylium ion containing fluorine, which is attributed to chlorine-fluorine exchange, as described in Equation (2).

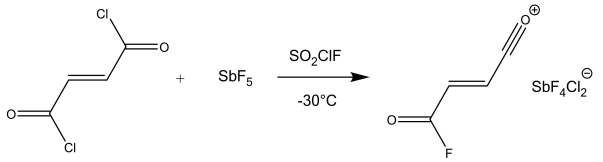

(2)

Avoiding the chlorine-fluorine exchange we chose $SbCl_5$ in liquid SO_2ClF to further analyze the Lewis basic characteristics of $C_4H_2Cl_2O_2$. This reaction resulted in a diadduct with O-coordinated $SbCl_5$ (see Equation (3)). However, neither the formation of monoacyl cations nor of diacylium ions was observed, using fumaryl chloride and the Lewis acid $SbCl_5$ as starting materials.

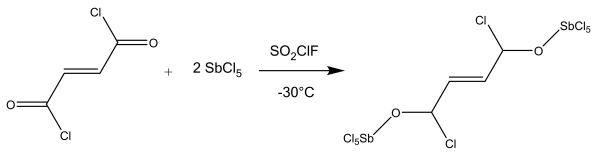

(3)

All of the reactions were performed at −30 °C. Excess SO_2ClF, which served as a solvent, was removed in a dynamic vacuum at −78 °C. The colorless salts $[C_4H_2FO_2]^+[Sb_3F_{16}]^-$ **(1)** and $[C_4H_2FO_2]^+[SbCl_2F_4]^-$ **(2)** are stable up to 20 °C. The light yellowish crystals of $C_4H_2Cl_2O_2 \cdot 2\ SbCl_5$ **(3)** decompose above 5 °C.

Crystal structure of $[C_4H_2FO_2]^+[Sb_3F_{16}]^-$

The monoacylium ion of fumaryl fluoride $[C_4H_2FO_2]^+[Sb_3F_{16}]^-$ **(1)** crystallizes in the monoclinic space group $P2_1/c$ with four formula units per unit cell. The asymmetric unit of **1** is depicted in Figure 1. Associated selected bond lengths and angles are summarized in Table 1.

As the monoacyl cation exists as *trans* conformer, we compare the bond lengths and angles to the *trans-trans* conformer of fumaryl fluoride.[9] The fluoride abstraction affects

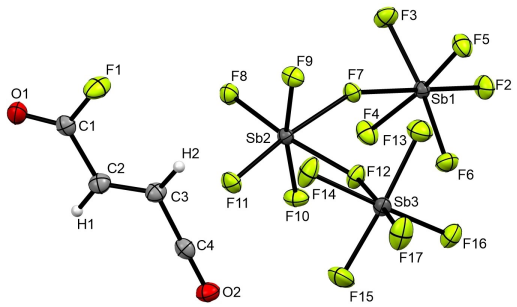

Figure 1. Asymmetric unit of $[C_4H_2FO_2]^+[Sb_3F_{16}]^-$ (displacement ellipsoids with 50 % probability).

Table 1. Selected bond lengths and angles of $[C_4H_2FO_2]^+[Sb_3F_{16}]^-$ (1) with estimated standard deviations in parentheses. Symmetry operations: *i* = 2−*x*, 0.5+*y*, 0.5−*z*; *ii* = *x*, 1.5−*y*, −0.5+*z*; *iii* = 1+*x*, 1.5−*y*, −0.5+*z*; *iv* = 1+*x*, *y*, *z*.

Bond lengths [Å]			
C1–F1	1.328(3)	C2–C3	1.310(5)
C1–O1	1.169(5)	C3–C4	1.416(5)
C1–C2	1.481(5)	C4–O2	1.104(4)
Bond angles [°]			
F1–C1–O1	121.7(3)	C1–C2–C3	122.1(4)
F1–C1–C2	112.4(3)	C2–C3–C4	118.2(4)
O1–C1–C2	126.0(3)	C3–C4–O2	178.9(4)
Angles of torsion [°]			
C1–C2–C3–C4	−178.8(3)	C3–C2–C1–O1	175.9(4)
C3–C2–C1–F1	−5.2(5)		
Intermolecular contacts [Å]			
C4···F11	2.758(4)	C4···O1*i*	2.811(4)
C4···F13*ii*	2.917(4)	C4···F2*iii*	2.786(4)
C3–H2···F4*iv*	3.155(5)		

considerably the remaining C≡O bond length. Compared to the starting material,[9] the C4–O2 bond distance is with 1.104(4) Å significantly reduced and in the range between formal double (1.19 Å) and formal triple bonds (1.07 Å).[8] The C≡O bond length in **1** agrees well with the values of reported acylium ions in the literature.[10–12] The comparison of the structural parameters of the acylium ion side of $[C_4H_2FO_2]^+$ with these of fumaronitrile is appropriate due to their isoelectronicity. Hence, we examined the crystal structure of fumaronitrile $C_4H_2N_2$ which crystallizes in the monoclinic space group with two formula units per unit cell. The formula unit of $C_4H_2N_2$ is depicted in Figure S1 and the corresponding selected bond lengths and angles are summarized in Table S1 in the Supporting Information. The C4–C3 bond distance in **1** is with 1.416(5) Å notably short, in particular when compared with the respective bond length of fumaronitrile (1.436(2) Å), where the carbon atom is sp-hybridized as well. The shortening of the carbon-carbon distance is in accordance with the corresponding values observed in the methyloxocarbonium ion.[11] In addition, the C–F bond distance (1.328(2) Å) is reduced by 0.021 Å compared to *trans-trans* fumaryl fluoride.[9] The strongest impact on the bond angles in **1** is observed for C3–C4–O2, which is widened by 51.7° to 178.9(4)°, revealing the linear structure of the acyl moiety. Furthermore, the C2–C3–C4 bond angle is reduced by 4.9° to 118.2(4)°. The slightly distorted planar structure of the $[C_4H_2FO_2]^+$ cation is based on the acyl fluoride moiety being twisted out of the carbon-skeleton plane by 5°.

The terminal Sb–F bond distances in the *cis*-fluorine-bridged $[Sb_3F_{16}]^-$ anion are in the range between 1.833(2) Å and 1.853(2) Å. The bridging Sb–F bond lengths are weaker than the terminal ones with up to 2.084(2) Å. Both, the terminal and the bridging bond distances are in agreement with reported values for $[Sb_3F_{16}]^-$ anions.[13–15] The Sb–F–Sb bond angles are with 151.0(1)° and 140.5(1)° in good accordance with the literature.[13–15] In the crystal packing of **1** different types of

Research Article
doi.org/10.1002/ejic.202200391

intermolecular contacts are formed, which are demonstrated in Figure 2.

The hydrogen bond C3–H2···F4*iv* (3.155(5) Å) is classified as moderate referred to the categorization of Jeffrey.[16] Aside from that, the crystal structure of **1** exhibits interactions between the cationic C4 atom tetracoordinated by nucleophilic fluorine and oxygen atoms. The distances C4···F11 (2.758(4) Å), C4···F13*ii* (2.917(4) Å) and C4···F2*iii* (2.786(4) Å) which are in accordance with other reported C···F contacts,[11,17–19] are below the sum of the van der Waals radii of 3.17 Å,[20] respectively. In addition, an interaction between the carbonyl group of one cation and the acylium ion side of another cation is observed, which is shown in Figure 2. The C4···O1*i* contact corresponds to reported carbonyl-carbonyl (C=O···C=O) interactions known in the literature.[21,22] With a distance of 2.811(4) Å it is below the sum of the van der Waals radii of 3.22 Å.[20] As can be seen in Figure 2, the carbonyl group is arranged above the acylium moiety in an L-shaped manner with an O2–C4···O1*i* dihedral angle of 94.4(2)°. The structural motif of the L-shape is established in the literature for carbonyl-carbonyl contacts.[22]

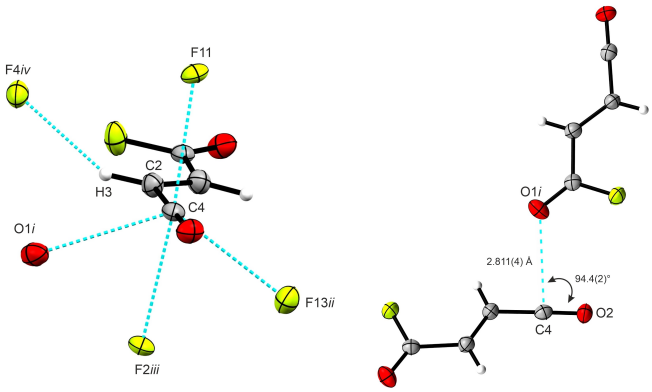

Figure 2. Left: Projection of the intermolecular contacts (drawn as dashed blue lines) in $[C_4H_2FO_2]^+[Sb_3F_{16}]^-$. Right: Illustration of the C=O···C=O interaction in $[C_4H_2FO_2]^+[Sb_3F_{16}]^-$ (displacement ellipsoids with 50% probability). Symmetry operations: *i* = 2−*x*, 0.5+*y*, 0.5−*z*; *ii* = *x*, 1.5−*y*, −0.5+*z*; *iii* = 1+*x*, 1.5−*y*, −0.5+*z*; *iv* = 1+*x*, *y*, *z*.

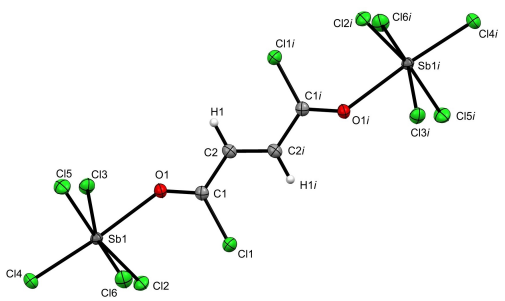

Figure 3. Formula unit of $C_4H_2Cl_2O_2 \cdot 2\ SbCl_5$ (displacement ellipsoids with 50% probability). Symmetry operation: *i* = 1−*x*, −*y*, 1−*z*.

Crystal structure of $C_4H_2Cl_2O_2 \cdot 2\ SbCl_5$

The diadduct of fumaryl chloride with $SbCl_5$ crystallizes in the orthorhombic space group *Pbca* with four formula units per unit cell. The formula unit of ($C_4H_2Cl_2O_2 \cdot 2\ SbCl_5$ **(3)**) is depicted in Figure 3 and selected structural parameters of the crystal structure of **3** are combined in Table 2.

In the solid state of the diadduct, fumaryl chloride exists as the *trans-trans* conformer. This is in accordance with reported crystal data of fumaryl chloride, revealing exclusively the thermodynamically preferred *trans-trans* conformer.[9,23,24] The donor-acceptor complex is based on the formation of Sb–O bonds. A lone pair of electrons is shared by the oxygen atom of the acyl chloride moiety with the metal of the Lewis acid. The Sb1–O1 bond length is with 2.359(2) Å longer than formal Sb–O bond distances (2.02 Å).[8] However, this bond length is in good agreement with reported values in the literature of other O-coordinated complexes like $SbCl_5 \cdot CH_3C_6H_4COCl$ (2.253(6) Å)[25] and 2 $SbCl_5 \cdot ClOCCH_2CH_2COCl$ (2.428 Å).[12] The coordination of $SbCl_5$ to the acyl chloride group leads to significant elongation of the C=O bond lengths in **3** (C1–O1 1.220(3) Å) in comparison with the starting material (1.191(2) Å).[23] Given that the C=O bond distances are increased, the C–Cl bond lengths are with 1.712(3) Å (C1–Cl1) significantly reduced compared to that in fumaryl chloride (1.783(2) Å).[23] The C=C double and C–C single bonds are not affected by the formation of the donor-acceptor complex. The value of 140.1(2)° observed for the Sb1–O1–C1 bond angle is in accordance with that determined for 2 $SbCl_5 \cdot ClOCCH_2CH_2COCl$ (143.6°).[12] The variation from the expected angle of 120° for sp^2-hybridized oxygen atom refers to intramolecular steric effects.[25] The bond angle Cl1–C1–C2 is widened by 3.3°, whereas the O1–C1–C2 is reduced by 5.5° in contrast to the educt.[23] Antimony is coordinated by six atoms forming an octahedral structure. The bond angles of the $SbCl_5O$

Table 2. Selected bond lengths and angles of $C_4H_2Cl_2O_2 \cdot 2\ SbCl_5$ **(3)** with estimated standard deviations in parentheses. Symmetry operations: *i* = 1−*x*, −*y*, 1−*z*; *ii* = 1−*x*, −0.5+*y*, 0.5−*z*, *iii* = 0.5−*x*, −0.5+*y*, *z*.

Bond lengths [Å]	
C1–Cl1	1.712(3)
C1–O1	1.220(3)
C1–C2	1.472(4)
C2–C2*i*	1.326(3)
Sb1–O1	2.359(2)
Bond angles [°]	
O1–C1–Cl1	122.0(2)
Cl1–C1–C2	117.9(2)
O1–C1–C2	120.0(2)
C1–C2–C2*i*	123.6(2)
Sb1–O1–C1	140.1(2)
Angles of torsion [°]	
C1–C2–C2*i*–C1*i*	−180.0(2)
O1–C1–C2–C2*i*	−172.5(2)
Cl1–C1–C2–C2*i*	6.9(3)
Intermolecular contacts [Å]	
C1···Cl4*iii*	3.301(3)
Cl2*i*···Cl5*ii*	3.305(1)

Research Article
doi.org/10.1002/ejic.202200391

moiety of **3** deviate up to 15° from the ideal angles indicating a distortion of the coordination polyhedra, which arises from the difference in the size of the ligands. The Sb–Cl bond lengths range between 2.314(1) Å and 2.340(1) Å, which are slightly shorter than formal Sb–Cl bond distances (2.38 Å).[8] These values comply with other reported values for $SbCl_5$ adducts.[25,26] The complexes are connected with each other via two different intermolecular contacts, which are illustrated in Figure 4. The distance C1···Cl4*iii* (3.301(3) Å) is below the sum of the van der Waals radii of 3.45 Å.[20] The halogen-halogen contact, Cl2*i*···Cl5*ii*, is with 3.305(1) Å below the sum of the van der Waals radii of 3.50 Å[20] and consonant with reported Cl···Cl interactions.[27] The attractive attribute of this contact arises in the electrostatic potential around the chlorine atom, being not completely negative but holding a small positive area. The other chlorine atom can be attracted by this region.[28]

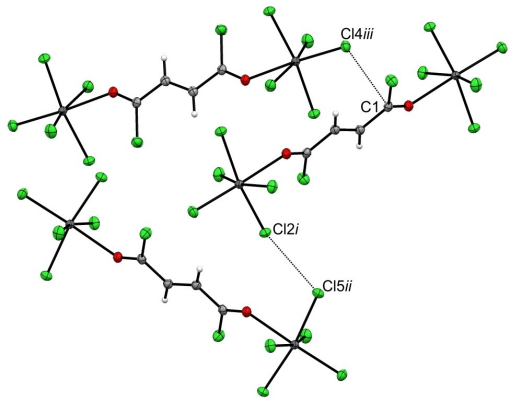

Figure 4. Projection of the intermolecular contacts in $C_4H_2Cl_2O_2 \cdot 2\ SbCl_5$ (displacement ellipsoids with 50% probability). Symmetry operations: *i* = 1−*x*, −*y*, 1−*z*; *ii* = 1−*x*, −0.5+*y*, 0.5−*z*, *iii* = 0.5−*x*, −0.5+*y*, *z*. Intermolecular contacts are drawn as dashed lines.

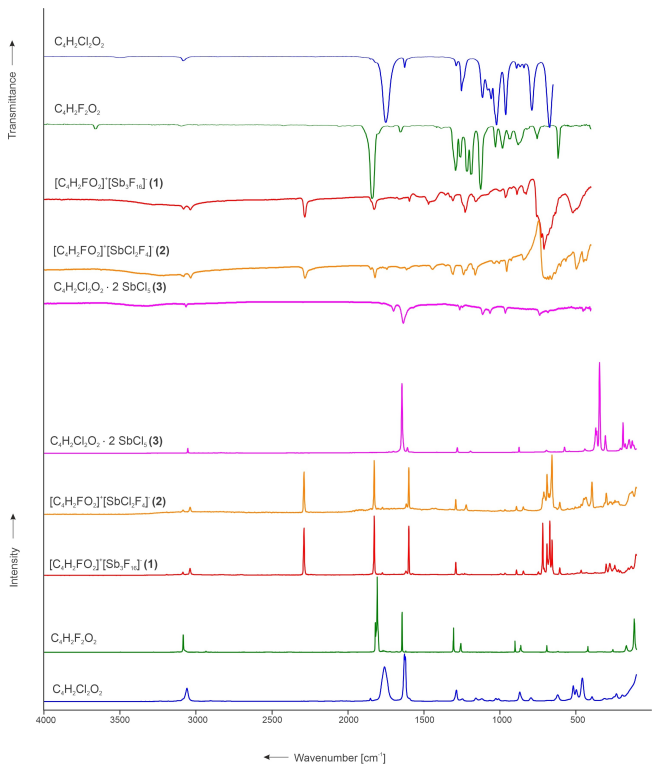

Figure 5. Low-temperature IR and Raman spectra of fumaryl chloride,[9] fumaryl fluoride,[9] $[C_4H_2FO_2]^+[Sb_3F_{16}]^-$, $[C_4H_2FO_2]^+[SbCl_2F_4]^-$ and $C_4H_2Cl_2O_2 \cdot 2\ SbCl_5$.

Vibrational spectra of $[C_4H_2FO_2]^+[Sb_3F_{16}]^-$ and $[C_4H_2FO_2]^+[SbCl_2F_4]^-$

The low-temperature vibrational spectra of $[C_4H_2FO_2]^+[Sb_3F_{16}]^-$ **(1)**, $[C_4H_2FO_2]^+[SbCl_2F_4]^-$ **(2)**, $C_4H_2Cl_2O_2 \cdot 2\ SbCl_5$ **(3)** and fumaryl chloride[9] together with crystalline fumaryl fluoride[9] are shown in Figure 5. Table 3 displays selected experimental vibrational frequencies of **1** and **2** combined with the quantum chemically calculated frequencies of the cation $[C_4H_2FO_2]^+$. The entire table (Table S2) is enclosed in the Supporting Information.

The monoacyl cation reveals a *trans* conformational structure in the crystalline form, as mentioned in the section above. Due to the abstraction of one halogen atom, the monoacylium ion is expected to have C_s point symmetry with the vibrational modes comprising the irreducible representations 15 *A′*+6 *A″*, where all modes are IR and Raman active. The vibrational frequencies were assigned by analyzing the Cartesian displacement vectors of the calculated vibrational modes of $[C_4H_2FO_2]^+$. The successful formation of the oxocarbenium ion is confirmed by the occurrence of the C≡O stretching vibration in the IR spectra at 2284 cm^{-1} **1**, **2** and in the Raman spectra at 2289 cm^{-1} **1**, **2**. The vibration of the remaining carbonyl group leads to a band in the IR spectra (1828 cm^{-1} **1**, 1821 cm^{-1} **2**) and a strong line in the Raman spectra (1826 cm^{-1} **1**, **2**), which are in good agreement with the C=O stretching vibrations of the educt[9] and confirms the appearance of monoacylium ions. The C–H stretching vibrations of the acylium ion side are red-shifted up to 61 cm^{-1} compared to the neutral compound[9] and occur in the IR spectra at 3038 cm^{-1} **1**, 3036 cm^{-1} **2**, respectively, and in the Raman spectra at 3039 cm^{-1} **1**, 3038 cm^{-1} **2**, respectively. The C–C stretching mode appearing in the Raman spectra at 995 cm^{-1} **1**, **2** is blue-shifted by 133 cm^{-1} compared to the ν_s(C–C) of fumaryl fluoride.[9] The decrease of this C–C single bond distance is in compliance with the crystal data of **1**. The C–Cl stretching vibrations in the spectra of fumaryl chloride[9] at 673 cm^{-1} (IR) and at 619 cm^{-1} (Ra), which are in agreement with the literature[24] are not detectable in the vibrational spectra of **2**. Instead, in the Raman spectrum of **2** a line arises at 1290 cm^{-1}, which is also observed in the Raman spectrum of **1**. This line is assigned to a C–F bond. We, therefore, assume a chlorine-fluorine exchange for the reaction of fumaryl chloride with the Lewis acid SbF_5, as it is described above in Equation (2). This halogen exchange between alkyl chlorides and SbF_5 giving alkyl fluorides combined with antimony chlorofluorocations is hardly reported in the literature.[29] Comparing the stretching mode of the C–F bond of **1** and **2** with the symmetric C–F stretching vibration of the neutral compound[9] it is blue-shifted by 33 cm^{-1}, which

Research Article
doi.org/10.1002/ejic.202200391

Chemistry Europe
European Chemical Societies Publishing

Table 3. Selected experimental vibrational frequencies [cm^{-1}] of $[C_4H_2FO_2]^+[Sb_3F_{16}]^-$ **(1)**, $[C_4H_2FO_2]^+[SbCl_2F_4]^-$ **(2)** and calculated vibrational frequencies [cm^{-1}] of $[C_4H_2FO_2]^+$.

$[C_4H_2FO_2]^+[Sb_3F_{16}]^-$ **(1)** exp.[a]		$[C_4H_2FO_2]^+[SbCl_2F_4]^-$ **(2)** exp.[a]		$[C_4H_2FO_2]^+$ calc.[b]	Assignment		
IR	Raman	IR	Raman	IR/Raman			
3082 m	3085 (6)	3080 vs	3085 (7)	3194 (20/41)	ν_1	A'	ν(C–H)
3038 m	3039 (12)	3036 vs	3038 (12)	3152 (73/52)	ν_2	A'	ν(C–H)[c]
2284 m	2289 (80)	2284 vs	2289 (72)	2327 (579/153)	ν_3	A'	ν(C≡O)[c]
1828 m	1826 (100)	1821 vs	1826 (91)	1876 (155/187)	ν_4	A'	ν(C=O)
1595 w	1599 (83)	1599 vs	1599 (79)	1612 (150/115)	ν_5	A'	ν(C=C)
1310 w	1290 (22)	1308 vs	1290 (25)	1214 (225/9)	ν_8	A'	ν(C–F)
1001 w	995 (3)	1005 s	995 (7)	1022 (44/2)	ν_9	A'	ν(C–C)[c]
962 w	966 (4)	955 vs	966 (8)	1010 (30/1)	ν_{16}	A''	γ(HCCH)
837 w	846 (8)	845 s	846 (13)	884 (38/10)	ν_{10}	A'	ν(C–C)
	605 (13)	602 s	605 (21)	676 (20/4)	ν_{11}	A'	δ(COF)

[a] Abbrevations for IR intensities: v = very, s = strong, m = medium, w = weak. IR intensities in km/mol; Raman intensities in $Å^4$/u. Experimental Raman activities are relative to a scale of 1 to 100. [b] Calculated on the B3LYP/aug-cc-pVTZ level of theory. [c] acylium ion side.

agrees well with the shortening of the C–F bond length in the crystal structure of **1**. The vibrational frequencies attributed to the $[Sb_3F_{16}]^-$ anion in **1** conform to reported data in the literature.[13,14,30] The lines and bands assigned to the chlorofluoroantimonate(v) anion $[SbCl_2F_4]^-$ in the spectra of **2** are in accordance with reported data.[31]

Vibrational spectra of $C_4H_2Cl_2O_2 \cdot 2\ SbCl_5$

The low-temperature vibrational spectra of $C_4H_2Cl_2O_2 \cdot 2\ SbCl_5$ **(3)** and fumaryl chloride[9] are shown in Figure 5. Selected experimental vibrational frequencies of **3** together with the quantum chemically calculated frequencies of the donor-acceptor complex $C_4H_2Cl_2O_2 \cdot 2\ SbCl_5$ are given in Table 4. The Supporting Information holds the entire table (Table S3).

Table 4. Selected experimental vibrational frequencies [cm^{-1}] and calculated vibrational frequencies [cm^{-1}] of $C_4H_2Cl_2O_2 \cdot 2\ SbCl_5$.

$C_4H_2Cl_2O_2 \cdot 2\ SbCl_5$ **(3)** exp.[a]		$C_4H_2Cl_2O_2 \cdot 2\ SbCl_5$ calc.[b]	Assignment		
IR	Raman	IR/Raman			
3067 w		3225(11/0)	ν_{43}	B_u	ν_{as}(C–H)
	3054 (5)	3225(0/49)	ν_1	A_g	ν_s(C–H)
	1644 (77)	1792(0/1589)	ν_2	A_g	ν_s(C=O)
1635 vs		1782(1611/0)	ν_{44}	B_u	ν_{as}(C=O)
	1607 (6)	1735(0/361)	ν_3	A_g	ν(C=C)
	1193 (2)	1213(0/72)	ν_5	A_g	ν_s(C–C)
1113 m		1135(444/0)	ν_{46}	B_u	ν_{as}(C–C)
739 s		753(159/0)	ν_{47}	B_u	ν_{as}(C–Cl)
	693 (3)	692(0/10)	ν_6	A_g	ν_s(C–Cl)
	441 (5)	437(0/9)	ν_8	A_g	ν_s(Sb–O)
442 w	368 (28)	394(0/53)	ν_9	A_g	ν_s(Sb–Cl)
413 w		393(189/0)	ν_{50}	B_u	ν_{as}(Sb–Cl)
	361 (24)	385(0/1)	ν_{10}	A_g	ν_s(Sb–Cl_2)
	344 (100)	353(0/104)	ν_{11}	A_g	ν_s(Sb–Cl_4)
	306 (19)	304(0/18)	ν_{35}	B_g	ν_s(Sb–Cl_4)

[a] Abbrevations for IR intensities: v = very, s = strong, m = medium, w = weak. IR intensities in km/mol; Raman intensities in $Å^4$/u. Experimental Raman activities are relative to a scale of 1 to 100. [b] Calculated at the M06-2X/aug-cc-pVTZ level of theory and Sb was calculated at the M06-2X/GenECP MWB46 level.

In the crystal structure of **3** fumaryl chloride reveals a *trans-trans* conformational arrangement, which was taken into account in the calculation of the local minimum structure of $C_4H_2Cl_2O_2 \cdot 2\ SbCl_5$. The simulation of the donor-acceptor complex was performed by employing the density functional M06-2X, which performs better than B3LYP in molecules, where dispersion interactions contribute.[32] A comparison of the experimental data of **3** with the calculated structural parameters and vibrational frequencies conducted by the density functionals B3LYP and M06-2X is listed in the Supporting Information (Table S4 and S5). The values obtained from the calculation at the M06-2X/aug-cc-pVTZ level of theory are overall in good agreement with the experimental parameters. For the antimony atoms the quasi-relativistic effective core potential MWB46 was applied. The diadduct $C_4H_2Cl_2O_2 \cdot 2\ SbCl_5$ is assumed to have C_{2h} point symmetry with 60 fundamental vibrations ($19\ A_g + 12\ A_u + 11\ B_g + 18\ B_u$). On account of the inversion center, the rule of mutual exclusion[33] applies to the diadduct. The assignment of the vibrational frequencies was performed by examining the Cartesian displacement vectors of the calculated vibrational modes of $C_4H_2Cl_2O_2 \cdot 2\ SbCl_5$. The coordinative Sb–O bond connecting the Lewis acid with fumaryl chloride has notable influence on the C=O stretching vibration, appearing in the IR spectrum at 1635 cm^{-1} and in the Raman spectrum at 1644 cm^{-1}. In comparison with the starting material,[24] the C=O stretching modes are red-shifted up to 127 cm^{-1}, which is in good agreement with reported vibrational frequencies of other complexes like $SbCl_5 \cdot C_6H_5COCl$.[34] The weakening of the C=O bonds, which is confirmed by the crystal data, indicates that **3** consists mostly of polarized donor-acceptor complexes.[34] The C–Cl stretching mode appearing in the Raman spectrum at 693 cm^{-1} and in the IR spectrum at 739 cm^{-1} is blue-shifted by up to 67 cm^{-1} compared to fumaryl chloride.[24] The shortening of the C–Cl bond distance is in accordance with the crystal data of **3**. The ν_s(Sb–O), observed in the Raman spectrum at 441 cm^{-1}, is red-shifted in comparison with formal Sb–O vibrational frequencies.[33] The detection of the weak Sb–O bond is in compliance with the crystal structure. The Sb–Cl stretching vibrations arise in the range between

Research Article
doi.org/10.1002/ejic.202200391

368 cm^{-1} and 306 cm^{-1}, which are in agreement with reported vibrational frequencies of other oxonium adducts of $SbCl_5$.[35]

Quantum chemical calculations

The structure of $[C_4H_2FO_2]^+$ was calculated at the B3LYP/aug-cc-pVTZ level of theory. A comparison of the single-crystal X-ray structure of **1** and the calculated structure of $[C_4H_2FO_2]^+$ along with bond lengths and angles is displayed in Figure 6.

The values obtained from the calculation are overall in good agreement with the experimental parameters. However, the C2–C3 bond length is overestimated whereas the C3–C4 is even underestimated by the calculation. The discrepancy in these values arises presumably from the intermolecular contacts in the crystal structure of **1**, which are not taken into account in the calculation. To examine the properties of these interactions, the electrostatic potential (ESP) map in combination with natural population analysis (NPA) charges of the $[C_4H_2FO_2]^+$ cation were calculated. Figure 7 illustrates the C···O and C···F

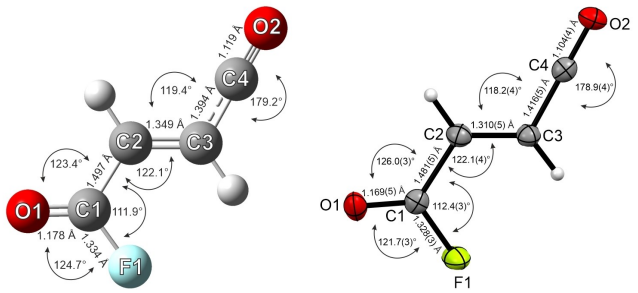

Figure 6. Calculated (left) and experimental (right) structures of $[C_4H_2FO_2]^+$ including bond lengths and angles.

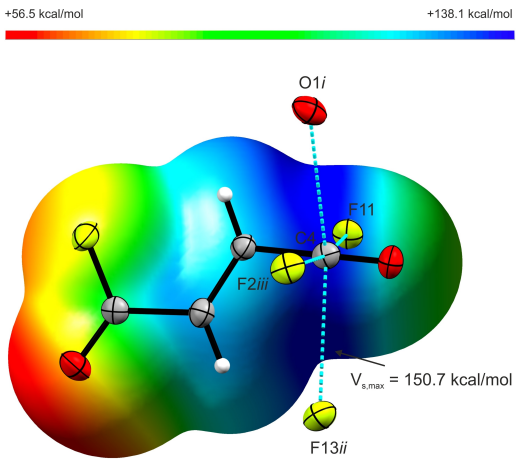

Figure 7. Intermolecular interactions in the crystal structure of **1** (displacement ellipsoids with 50% probability). C···O and C···F contacts are drawn as dashed blue lines. The calculated ESP surface mapped onto an electron density isosurface value of 0.0004 $bohr^{-3}$ with the color scale range from 56.5 kcal mol^{-1} to 138.1 kcal mol^{-1}. Symmetry operations: *i* = 2−*x*, 0.5+*y*, 0.5−*z*; *ii* = *x*, 1.5−*y*, −0.5+*z*; *iii* = 1+*x*, 1.5−*y*, −0.5+*z*.

contacts along with the ESP map. The ESP map in company with the NPA charges of $[C_4H_2FO_2]^+$ is shown in Figure 9. In the ESP map of the monoacyl cation, the negative charge density is concentrated at the oxygen atom O1 of the acyl fluoride group, as indicated by the red surface. The region around the sp-hybridized carbon atom suffers from a depletion of electron density and provides a positive electrostatic potential, which is observed in the ESP map. This is in accordance with the high positive NPA charge of the C4 atom of the monoacyl cation. Such a region of density depletion and positive electrostatic potential are designated in the literature as π-hole,[36,37] illustrated in the ESP map as the dark blue area around the C4 atom. The magnitude of the π-hole, quantified by the $V_{S,max}$ parameter, amounts to 150.7 kcal mol^{-1}. Approaching this positive π-hole is accordingly self-evident for nucleophiles,[36] such as the $[Sb_3F_{16}]^-$ anion and the negatively polarized O1 atom of the acyl fluoride moiety. The interaction of the latter with the π-hole generates the C4···O1*i* contact with a distance of 87% of the sum of the van der Waals radii.[20] Three carbon-fluorine contacts are additionally built, originating from the π-hole to the $[Sb_3F_{16}]^-$. The C4···F distances range from 87% to 92% of the sum of the van der Waals radii.[20] Hence, the positive charge on the C4 atom is stabilized by electrostatic attraction.[38,39] In addition, orbital interactions reinforce the attractive interaction[39] between the acylium moiety and the nucleophiles. There are reported examples of sp^2-hybridized carbenium ions stabilized by fluorine bridging along the axis of the unoccupied p_z orbital.[17–19] However, in the monoacyl cation the corresponding carbon atom is supposed to be sp-hybridized. To confirm the assumption of the sp-hybridization of the C4 atom, natural bond orbital calculations of $[C_4H_2FO_2]^+$ were performed. In addition, a deeper understanding of the intermolecular interactions concerning the C4 atom is expected from the calculations. The bonding and antibonding orbitals with the participation of the C4 atom are illustrated in Figure 8. To confirm the sp-hybridization, the corresponding p-orbitals are examined. One σ-bond between C4 and C3 is formed, comprising 41.1% p-character of C4. Another σ-bond between C4 and O2 contains 58.5% p-character of C4. There are two π-bonds formed between C4 and O2, consisting each of 99.8% p-character of C4, respectively. Therefore we conclude that the C4 atom is sp-hybridized and both p-orbitals are occupied and participate in the π-bonds to the O2 atom. In Table S6 in the Supporting Information, selected NBOs, regarding the acylium moiety, are summarized in combination with calculated values for electron occupancy, s-and p-character, and energy. The π-hole can be considered as positive electrostatic potential on unpopulated π* orbitals, which are thereby able to interact with electron donors.[40] Typically the regions of positive electrostatic potential are located perpendicular to the molecular framework.[38] In our case, the carbon atom is sp-hybridized leading to a π-hole formed in a ring structure around the carbon atom, representing a peculiarity of the acylium group. Concerning the C4–O2 bond in terms of bonding and antibonding orbitals, to gain a deeper understanding of the orbitals involved in the noncovalent interactions. Due to the π_z*(C4–O2) orbital being orientated towards the electron

Research Article
doi.org/10.1002/ejic.202200391

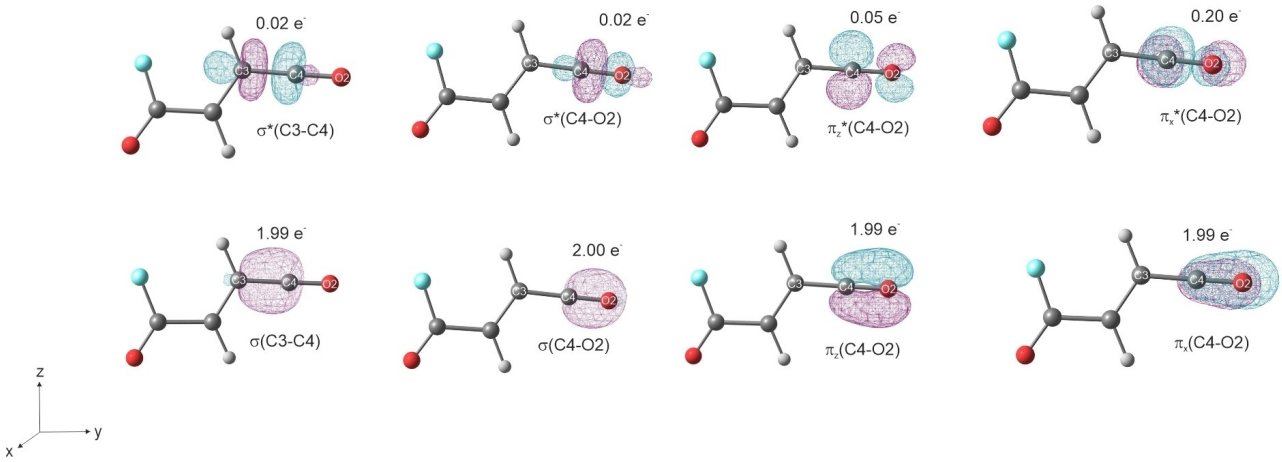

Figure 8. Selected NBOs for the C3–C4 and C4–O2 bonds with associated occupancies of $[C_4H_2FO_2]^+$.

donors O1*i* and F13*ii*, their lone pairs can delocalize into the antibonding orbital. The π_x*(C4–O2) is populated by the lone pairs of F11 and F2*iii*, because it is arranged towards these ligands. To summarize, we can say that the highly electron-deficient oxocarbenium center, which is associated with a π-hole providing a ring structure, is stabilized by electrostatic attraction[38,39] and electron back-donation[18,41] from one oxygen and three fluorine ligands (lp→π*(C4–O2)). The stabilization effect is confirmed by the high stability of the acylium salts **1** and **2** up to 20 °C.

Aside from that, we were interested in analyzing the electron distribution and charge-related properties of the diacyl cation $[C_4H_2O_2]^{2+}$, which cannot be formed even with the employment of large excess of SbF_5. Hence, calculations of the ESP map including NPA charges were performed. Figure 9 shows a comparison of the ESP maps along with the NPA charges of $[C_4H_2FO_2]^+$ and of $[C_4H_2O_2]^{2+}$. In the same way, as it is observed in the ESP map of the monoacyl cation, the regions around the sp-hybridized carbon atoms hold a positive electrostatic potential in the ESP map of $[C_4H_2O_2]^{2+}$. This is consonant with the high positive NPA charges of the C1 and C4 atoms of the diacyl cation. The ESP map of the diacyl cation shows a negative electrostatic potential located at the oxygen atoms. Compared to the O2 atom of $[C_4H_2FO_2]^+$ the negative NPA charges of O1 and O2 of the diacyl cation are decreased. In the ESP map of $[C_4H_2O_2]^{2+}$ the region along the C=C double bond holds a slightly positive charge density but negative NPA charges. The charge distribution providing only a small distance between the positive charges of C1 and C4 leads to repulsive effects. This represents the explanation for the inability to prepare the diacyl cation. In the literature this observation is known, as it is possible to prepare diacylium ions from diacyl fluorides FOC–$(CH_2)_n$–COF only for $n \geq 3$.[42-44] Certainly, the diprotonation of fumaryl fluoride is observed,[45] owning two positive charges as well, with the same distance between the charged centers. Compared to the diacyl cation the positive charges in the diprotonated species are distributed to a greater extent over the protonated acyl fluoride group, as it is illustrated in the calculated ESP map of the diprotonated fumaryl fluoride.[45] The diacyl cation, however, is characterized by a remarkable charge-charge repulsion, without the possibility of delocalization, as it is depicted in the ESP map in Figure 9. The same observation has been made with succinyl fluoride and succinic acid.[43,44,46] Charge-charge repulsive effects prevent the formation of the diacyl cation of succinyl fluoride and the delocalization of the positive charges enables the formation of the diprotonated succinic acid.[43,44,46]

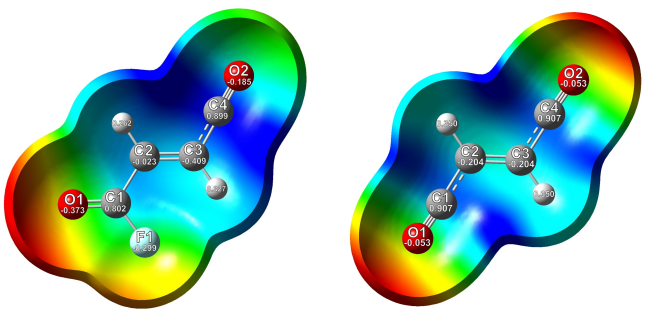

Figure 9. Left: Calculated ESP surface mapped onto an electron density isosurface value of 0.0004 $bohr^{-3}$ with the color scale range from 56.5 kcal mol^{-1} (red) to 138.1 kcal mol^{-1} (blue) of $[C_4H_2FO_2]^+$. Right: Calculated ESP surface mapped onto an electron density isosurface value of 0.0004 $bohr^{-3}$ with the color scale range from 169.4 kcal mol^{-1} (red) to 251.0 kcal mol^{-1} (blue) of $[C_4H_2O_2]^{2+}$. The NPA charges are given in a. u.

Conclusions

The key intermediates of the first step of the Friedel-Crafts acylation were synthesized by reacting fumaryl halides with different Lewis acids. The reaction of fumaryl fluoride with the Lewis acid SbF_5 in SO_2ClF solutions results in the formation of the monoacyl cation $[C_4H_2FO_2]^+$. Surprisingly, the monoacyl cation containing fluorine concerning the salt $[C_4H_2FO_2]^+$ $[SbCl_2F_4]^-$ was obtained for the reaction of fumaryl chloride

Research Article
doi.org/10.1002/ejic.202200391

with SbF_5 in SO_2ClF due to chlorine-fluorine exchange. Furthermore, the reaction of fumaryl chloride with $SbCl_5$ in SO_2ClF was examined. The covalent donor-acceptor complex $C_4H_2Cl_2O_2 \cdot 2\ SbCl_5$ was formed, containing the oxygen-bonded Lewis acids. The compounds were isolated and characterized by low-temperature vibrational spectroscopy. Single-crystal X-ray structure analyses were undertaken for $[C_4H_2FO_2]^+[Sb_3F_{16}]^-$ and for $C_4H_2Cl_2O_2 \cdot 2\ SbCl_5$. To interpret the experimental results, quantum chemical calculations were performed for $[C_4H_2FO_2]^+$ on the B3LYP/aug-cc-pVTZ and for $C_4H_2Cl_2O_2 \cdot 2\ SbCl_5$ on the M06-2X/aug-cc-pVTZ level of theory. In the crystal structure of $[C_4H_2FO_2]^+[Sb_3F_{16}]^-$ one C···O and three C···F contacts are observed and the origin of these interactions is investigated with the help of ESP maps, NPA charges, and NBO analysis. A ring-shaped π-hole is formed around the oxocarbenium center, due to the sp-hybridization of the carbon atom. The positive charge is stabilized by electrostatic attraction and electron back-donation from the ligands ($lp \rightarrow \pi^*(C{\equiv}O)$). In addition, calculations of ESP maps including NPA charges for the diacyl cation $[C_4H_2O_2]^{2+}$ were executed. Small distances between the positive charges involving charge-charge repulsion elucidate why the formation of the diacyl cation cannot be observed. The observation that fumaryl chloride, as well as fumaryl fluoride, would not give diacylium ions can be considered as benefit for the Friedel-Crafts synthesis of ketones proving an acyl fluoride group because fluorine substituents are a common and essential drug component.

Experimental Section

Caution! Any contact with the components must be avoided. Be aware that the hydrolysis of SbF_5 and the reported salts might release HF, burning skin, and cause irreparable injury. Adequate safety precautions must be undertaken when using and handling these materials.

Apparatus and materials: All reactions were conducted by using standard Schlenk techniques with an electropolished stainless-steel vacuum line. Transparent FEP/PFA-reactors combined with stainless-steel valves were employed for the syntheses. The vacuum line and the reactors were dried with fluorine, before use. Excess fluorine was removed in a dynamic vacuum and absorbed by Sodalime. Antimony pentafluoride was managed in a Duran glass high vacuum line exerting Young valves. Low-temperature Raman spectroscopic measurements were performed in a glass cell under vacuum cooled down to −196 °C on a Bruker MultiRAMII FT-Raman spectrometer with Nd:YAG laser excitation ($\lambda = 1064$ nm). For the IR measurements, the respective sample was put on a CsBr single-crystal plate in a cooled cell. A Bruker Vertex-80 V-FT-IR spectrometer was employed for recording the low-temperature IR spectra. The low-temperature single-crystal X-ray diffractions of **1** and **3** were performed on an Oxford XCalibur3 diffractometer equipped with a Spellman generator (50 kV, 40 mA) and a Kappa CCD-detector, operating with Mo$K\alpha$ radiation ($\lambda = 0.71073$ Å). Data collection and reduction were executed using the program CrysAlisPro 1.171.38.46 (Rigaku OD, 2015).[47] The crystal structures were solved using SHELXT[48] and SHELXL-2018/3[49] of the WINGX software package.[50] The structures were checked by employing the software PLATON.[51] The absorption correction was carried out with the help of the SCALE3 ABSPACK multiscan method.[52] Selected data and parameters of the reported single-crystal structures **1**, **3**, and fumaronitrile are listed in Table S7 (Supporting Information). Quantum chemical calculations were performed on the B3LYP/aug-cc-pVTZ, M06-2X/aug-cc-pVTZ levels of theory and for Sb the basis set GenECP was applied using the software package Gaussian 09[53], and Gaussian16.[54] GaussView 6.0 was employed for the visualization and illustration of the ESP calculations.[55]

Syntheses of $[C_4H_2FO_2]^+[Sb_3F_{16}]^-$ (1) and $[C_4H_2FO_2]^+[SbCl_2F_4]^-$ (2): For **1**, the starting material, fumaryl fluoride, was prepared as previously reported, without further purification.[9] Antimony pentafluoride (540 mg, 2.5 mmol) was condensed at −196 °C into an FEP reactor vessel. Afterwards, for **1** fumaryl fluoride (100 mg, 0.8 mmol) and for **2** fumaryl chloride (230 mg, 1.5 mmol) were added under nitrogen atmosphere. Subsequently, 2 mL of SO_2ClF were condensed into the reactor vessel at −196 °C, respectively. The reaction mixture was warmed up to −30 °C and homogenized until the respective salts were completely dissolved. For crystallization of **1**, the reactor was left in an ethanol bath at −70 °C until the salts were recrystallized. For the vibrational measurements, the solvent SO_2ClF was removed in a dynamic vacuum at −78 °C. The compounds were obtained as colorless crystalline solids, stable up to 20 °C.

Synthesis of $C_4H_2Cl_2O_2 \cdot 2\ SbCl_5$ (3): Antimony pentachloride (598 mg, 2.0 mmol) and fumaryl chloride (153 mg, 1.0 mmol) were filled under a nitrogen atmosphere into an FEP reactor vessel. Accordingly, 2 mL of SO_2ClF were condensed into the reactor vessel at −196 °C. The reaction mixture was warmed up to −30 °C and homogenized until the compound was thoroughly dissolved. For crystallization, the reactor was left in an ethanol bath at -40 °C until the complex was recrystallized. For the vibrational measurements, the solvent SO_2ClF was removed in a dynamic vacuum at −78 °C. The compound was obtained as light yellowish crystals, which decompose above 5 °C.

Deposition Numbers 2155394 (for **1**), 2155395 (for **3**), and 2155396 (for fumaronitrile) contain the supplementary crystallographic data for this paper. These data are provided free of charge by the joint Cambridge Crystallographic Data Centre and Fachinformationszentrum Karlsruhe Access Structures service www.ccdc.cam.ac.uk/structures.

Acknowledgments

We gratefully acknowledge the financial support of the Department of Chemistry of the Ludwig-Maximilians-Universität München, the Deutsche Forschungsgemeinschaft (DFG) and the F-Select GmbH. Open Access funding is enabled and organized by Projekt DEAL. Open Access funding enabled and organized by Projekt DEAL.

Conflict of Interest

The authors declare no conflict of interest.

Data Availability Statement

The data that support the findings of this study are available in the supplementary material of this article.

Keywords: π-hole · acyl cations · $SbCl_5$ donor-acceptor complex · electrostatic potential maps · natural bond orbital analysis · Friedel-Crafts acylation intermediates · noncovalent interactions

[1] E. Kraka, D. Cremer, *Acc. Chem. Res.* **2010**, *43*, 59.
[2] E. K. Raja, D. J. DeSchepper, S. O. N. Lill, D. A. Klumpp, *J. Org. Chem.* **2012**, *77*, 5788.
[3] H. G. Frank, in *Industrial Aromatic Chemistry*, Springer, Berlin, **1988**.
[4] G. A. Olah, in *Friedel-Crafts and Related Reactions*, Wiley, New York, **1963**.
[5] J. K. Groves, *Chem. Soc. Rev.* **1972**, *1*, 73.
[6] a) Jie Jack Li, *Name Reactions. A Collection of Detailed Reaction Mechanisms*, Springer, Berlin, Heidelberg, **2006**; b) P. H. Gore, *Chem. Rev.* **1955**, *55*, 229.
[7] K. Müller, C. Faeh, F. Diederich, *Science* **2007**, *317*, 1881.
[8] A. F. Holleman, E. Wiberg, N. Wiberg, G. Fischer, in *Anorganische Chemie*, De Gruyter, Berlin, Boston, **2017**.
[9] M. C. Bayer, C. Jessen, A. J. Kornath, *Z. Anorg. Allg. Chem.* **2021**, *647*, 258.
[10] I. Bernhardi, T. Drews, K. Seppelt, *Angew. Chem. Int. Ed.* **1999**, *38*, 2232.
[11] F. P. Boer, *J. Am. Chem. Soc.* **1968**, *90*, 6706.
[12] J. M. Le Carpentier, R. Weiss, *Acta Crystallogr.* **1972**, *B28*, 1442.
[13] M. Gerken, D. A. Dixon, G. J. Schrobilgen, *Inorg. Chem.* **2002**, *41*, 259.
[14] R. Faggiani, D. K. Kennepohl, C. J. L. Lock, G. J. Schrobilgen, *Inorg. Chem.* **1986**, *25*, 563.
[15] A. J. Edwards, G. R. Jones, R. J. C. Sills, *Chem. Commun.* **1968**, 1527.
[16] G. A. Jeffrey, in *An introduction to hydrogen bonding, Topics in physical chemistry*, Oxford University Press, New York, **1997**.
[17] S. Beck, M. Feller, L. Spies, K. J. Dietrich, C. Jessen, K. Stierstorfer, A. J. Kornath, *ChemistryOpen* **2021**, *10*, 8.
[18] K. O. Christe, X. Zhang, R. Bau, J. Hegge, G. A. Olah, G. K. S. Prakash, J. A. Sheehy, *J. Am. Chem. Soc.* **2000**, *122*, 481.
[19] N. R. Götz, in *Ludwig-Maximilians-Universität, Diss.*, Universitätsbibliothek der Ludwig-Maximilians-Universität, München, **2011**.
[20] A. Bondi, *J. Phys. Chem.* **1964**, *68*, 441.
[21] W. Bolton, *Nature* **1964**, *201*, 987.
[22] B. Sahariah, B. K. Sarma, *Chem. Sci.* **2019**, *10*, 909.
[23] K. Hagen, *J. Mol. Struct.* **1985**, *128*, 139.
[24] J. M. Landry, J. E. Katon, *Spectrochim. Acta Part A* **1984**, *40*, 871.
[25] B. Chevrier, J. M. Le Carpentier, R. Weiss, *J. Am. Chem. Soc.* **1972**, *94*, 5718.
[26] L. Brun, C.-I. Brändén, *Acta Crystallogr.* **1966**, *20*, 749.
[27] V. R. Hathwar, T. N. Guru Row, *J. Phys. Chem. A* **2010**, *114*, 13434.
[28] S. Scheiner, *J. Phys. Chem. A* **2011**, *115*, 11202.
[29] J. Bacon, P. A. W. Dean, R. J. Gillespie, *Can. J. Chem.* **1971**, *49*, 1276.
[30] G. S. H. Chen, J. Passmore, *J. Chem. Soc. Dalton Trans.* **1979**, *8*, 1251.
[31] M. F. A. Dove, J. C. P. Sanders, *J. Chem. Soc. Dalton Trans.* **1992**, *23*, 3311.
[32] M. Walker, A. J. A. Harvey, A. Sen, C. E. H. Dessent, *J. Phys. Chem. A* **2013**, *117*, 12590.
[33] J. Weidlein, U. Müller, K. Dehnicke, in *Schwingungsspektroskopie*, Thieme, Stuttgart, **1988**.
[34] G. A. Olah, S. J. Kuhn, W. S. Tolgyesi, E. B. Baker, *J. Am. Chem. Soc.* **1962**, *84*, 14, 2733.
[35] M. Burgard, J. P. Brunette, M. J. F. Leroy, *Inorg. Chem.* **1976**, *15*, 1225.
[36] W. Zierkiewicz, M. Michalczyk, S. Scheiner, *Molecules* **2021**, *26*, 1740.
[37] H. Wang, W. Wang, W. J. Jin, *Chem. Rev.* **2016**, *116*, 5072.
[38] J. S. Murray, P. Lane, T. Clark, K. E. Riley, P. Politzer, *J. Mol. Model.* **2012**, *18*, 541.
[39] O. Loveday, J. Echeverría, *Nat. Commun.* **2021**, *12*, 5030.
[40] A. Bauzá, T. J. Mooibroek, A. Frontera, *ChemPhysChem* **2015**, *16*, 2496.
[41] T. Laube, *Chem. Rev.* **1998**, *98*, 1277.
[42] a) B. Chevrier, R. Weiss, *Angew. Chem. Int. Ed.* **1974**, *13*, 1; b) D. A. Klumpp, *Chem. Eur. J.* **2008**, *14*, 2004.
[43] J. W. Larsen, P. A. Bouis, *J. Am. Chem. Soc.* **1975**, *97*, 6094.
[44] G. A. Olah, M. B. Comisarow, *J. Am. Chem. Soc.* **1966**, *88*, 3313.
[45] M. C. Bayer, C. Kremser, C. Jessen, A. Nitzer, A. J. Kornath, *Chem. Eur. J.* **2022**, *28*, e202104422.
[46] G. A. Olah, A. M. White, *J. Am. Chem. Soc.* **1967**, *89*, 4752.
[47] Rigaku Oxford Diffraction, CrysAlisPro Software System, *Version 1.171.38.46*, Rigaku Corporation, Oxford, UK, **2015**.
[48] G. M. Sheldrick, *Acta Crystallogr.* **2015**, *A71*, 3.
[49] G. M. Sheldrick, *Acta Crystallogr.* **2015**, *C71*, 3.
[50] L. J. Farrugia, *J. Appl. Crystallogr.* **1999**, *32*, 837.
[51] A. L. Spek, *J. Appl. Crystallogr.* **2003**, *36*, 7.
[52] SCALE3 ABSPACK, *An Oxford Diffraction Program*, Oxford Diffraction Ltd, UK, **2005**.
[53] M. J. Frisch, G. W. Trucks, H. B. Schlegel, G. E. Scuseria, M. A. Robb, J. R. Cheeseman, G. Scalmani, V. Barone, B. Mennucci, G. A. Petersson, H. Nakatsuji, M. Caricato, X. Li, H. P. Hratchian, A. F. Izmaylov, J. Bloino, G. Zheng, J. L. Sonnenberg, M. Hada, M. Ehara, K. Toyota, R. Fukuda, J. Hasegawa, M. Ishida, T. Nakajima, Y. Honda, O. Kitao, H. Nakai, T. Vreven, J. A. Montgomery, Jr., J. E. Peralta, F. Ogliaro, M. Bearpark, J. J. Heyd, E. Brothers, K. N. Kudin, V. N. Staroverov, R. Kobayashi, J. Normand, K. Raghavachari, A. Rendell, J. C. Burant, S. S. Iyengar, J. Tomasi, M. Cossi, N. Rega, J. M. Millam, M. Klene, J. E. Knox, J. B. Cross, V. Bakken, C. Adamo, J. Jaramillo, R. Gomperts, R. E. Stratmann, O. Yazyev, A. J. Austin, R. Cammi, C. Pomelli, J. W. Ochterski, R. L. Martin, K. Morokuma, V. G. Zakrzewski, G. A. Voth, P. Salvador, J. J. Dannenberg, S. Dapprich, A. D. Daniels, O. Farkas, J. B. Foresman, J. V. Ortiz, J. Cioslowski, D. J. Fox, *Gaussian 09, Revision A.02*, Gaussian, Inc., Wallingford CT, **2009**.
[54] M. J. Frisch, G. W. Trucks, H. B. Schlegel, G. E. Scuseria, M. A. Robb, J. R. Cheeseman, G. Scalmani, V. Barone, G. A. Petersson, H. Nakatsuji, X. Li, M. Caricato, A. V. Marenich, J. Bloino, B. G. Janesko, R. Gomperts, B. Mennucci, H. P. Hratchian, J. V. Ortiz, A. F. Izmaylov, J. L. Sonnenberg, D. Williams-Young, F. Ding, F. Lipparini, F. Egidi, J. Goings, B. Peng, A. Petrone, T. Henderson, D. Ranasinghe, V. G. Zakrzewski, J. Gao, N. Rega, G. Zheng, W. Liang, M. Hada, M. Ehara, K. Toyota, R. Fukuda, J. Hasegawa, M. Ishida, T. Nakajima, Y. Honda, O. Kitao, H. Nakai, T. Vreven, K. Throssell, J. A. Montgomery, Jr., J. E. Peralta, F. Ogliaro, M. J. Bearpark, J. J. Heyd, E. N. Brothers, K. N. Kudin, V. N. Staroverov, T. A. Keith, R. Kobayashi, J. Normand, K. Raghavachari, A. P. Rendell, J. C. Burant, S. S. Iyengar, J. Tomasi, M. Cossi, J. M. Millam, M. Klene, C. Adamo, R. Cammi, J. W. Ochterski, R. L. Martin, K. Morokuma, O. Farkas, J. B. Foresman, D. J. Fox, *Gaussian 16, Revision A.03*, Gaussian, Inc., Wallingford CT, **2016**.
[55] R. Dennington, T. A. Keith, J. M. Millam, *GaussView, Version 6.0*, Semichem Inc., Shawnee Mission, **2016**.

Manuscript received: June 20, 2022
Revised manuscript received: July 1, 2022
Accepted manuscript online: July 4, 2022